Effect of heating rate and feedstock nature on electrical conductivity of biochar and biochar-based composites

Applications in Energy and Combustion Science 12 (2022) 100089

Contents lists available at ScienceDirect

Applications in Energy and Combustion Science

journal homepage: www.sciencedirect.com/journal/applications-in-energy-and-combustion-science

Effect of heating rate and feedstock nature on electrical conductivity of biochar and biochar-based composites

Mattia Bartoli [a,1], Maurizio Troiano [b,1], Paola Giudicianni [c,*], Davide Amato [c], Mauro Giorcelli [d], Roberto Solimene [c], Alberto Tagliaferro [d]

[a] Center for Sustainable Future Technologies, Italian Institute of Technology, Via Livorno 60, Turin 10144, Italy
[b] Dipartimento di Ingegneria Chimica, dei Materiali e della Produzione Industriale, Università Federico II di Napoli, p.le V. Tecchio, 80, 80125, Italy
[c] Istituto di Scienze e Tecnologie per l'Energia e la Mobilità Sostenibili – Consiglio Nazionale delle Ricerche, p.le V. Tecchio, 80, Naples 80125, Italy
[d] Dipartimento di Scienze e Tecnologia Applicate, Politecnico di Torino, 10129, Italy

ARTICLE INFO

Keywords:
Electrical conductivity
Biochar
Epoxy resin
Ash
Porosity
Polymer composite

ABSTRACT

Cost-effective strategies for integrating bio-oil production with biochar utilization in new sustainable platforms are needed to improve the economic viability of pyrolysis for energy applications. Recently, the use of biochar as filler in the preparation of polymer based composites received a great attention due to its ability to improve polymers mechanical, electrical and thermal properties.

This work aims to expand knowledge on the effect of the heating rate and feedstock chemical composition on the on the biochar structural and chemical characteristics affecting electrical properties of the biochar at different pyrolysis temperatures. Biochars were produced from three feedstocks, namely walnut shells (WS), the lignin rich residue from bio-ethanol production (LRR) and sewage sludge (SS), under slow and fast heating rate at 500, 600 and 700°C. The three feedstock differ for both the organic components (i.e. high lignin content in WS and LRR and presence of proteins in SS) and ash content which is highest in SS.

The produced biochars were characterized and the observed differences in their chemical and structural properties were discussed in relation to their effect on the measured electrical conductivity.

The severity of the pyrolysis treatment improved biochars electrical conductivity. Heating rate and feedstock type affected the electrical conductivity only marginally at 500 and 600°C, whereas at 700°C any relevant effect was observed. WS biochars produced at 500 and 600°C exhibited the lowest electrical conductivity regardless of the heating rate of the production process.

The biochars produced at 700°C were used to prepare epoxy resins composites. Despite their comparable conductive performance, the biochars lent different electrical conductivity to the composites depending on the biomass type and the heating rate experienced by the biomass samples during the pyrolytic treatment. The composite prepared with WS biochar produced under fast heating rate exhibited the highest electrical conductivity.

1. Introduction

Pyrolysis represents a viable option for the treatment of a wide variety of biomasses given its capability to function as a multiproduct provider (e.g., biofuels, bulk chemicals, bioenergy carriers, biomaterials). Even though technologies for bioenergy/biofuel production through fast pyrolysis are currently mature to enter the market [1], there is an urgent need to increase the economic feasibility of the whole production chain by developing cost-effective strategies to integrate bio-oil production for energy applications with bio-materials synthesis in new sustainable platforms [2]. In this framework, biochar, i.e. the solid product of the pyrolysis process, have physical and chemical characteristics that make it a bio-material with high performance potential in many applications [3].

In the last decades biochar attracted the interest of material scientists as carbon filler in polymer-based composites thanks to its ability to

* Corresponding author.
E-mail address: paola.giudicianni@stems.cnr.it (P. Giudicianni).
[1] First co-author.

https://doi.org/10.1016/j.jaecs.2022.100089
Received 30 November 2021; Received in revised form 31 May 2022; Accepted 4 October 2022
Available online 7 October 2022

improve the mechanical, thermal and optical properties of polymers [4] and to confer electrical conductivity to the polymer matrix [5]. Composites based on carbonaceous material and different polymers are widely used for thermal energy storage [7] and energy harvesting [8] as well as electrochemical sensors [9]. Energy storage devices (batteries, capacitors, fuel cells) are fundamental for the development of renewable energy by allowing energy to be captured, stored and transported whenever it is needed.

Carbon black [10], nanotubes [11] and graphene [12] were extensively studied in the past as composites fillers for this type of applications. However, despite their high performances, the high production costs and the use of fossil carbon sources hindered their large scale implementation. In this framework, the use of biochar, fits the twofold need of valorizing waste streams and using a renewable feedstock, thus contributing to promote the economic feasibility and the environmental sustainable production of composites.

The main issue with biochar utilization is the wide variability of its chemical and physical characteristics which greatly affect its electrical properties [13], thus representing one of the main obstacles for biochar application as filler in composites. The role of some biochar characteristics, such as presence of polar functional groups, aromatization and graphitization degree, ash content, porosity, in determining the evolution of the electrical characteristics as function of the pyrolysis temperature has been extensively studied and elucidated [14,15].

At very low carbonization temperature up to 400 °C, alternating current (AC) conductivity of carbonized wood and cellulose exhibited a decreasing trend with the temperature [14,15] due to the enhanced decomposition of the polar organic functional groups. At higher carbonization temperature an opposite trend was observed and the evolution of electric conductivity is mainly correlated with the sp2 hybridization of the carbon atoms. By rising the temperature an increasing number of carbon atoms with sp2 hybridization appears in polycondensed units, thus leading to the formation and growth of highly conducting carbon nanoclusters separated from regions of low conducting amorphous carbon. According to the two-phase composites model going through a percolation transition [16], the so-called quasi-percolation model [14], in the range 550-600°C the increase of AC conductivity of about an order of magnitude was observed due to the occurrence of electron hopping between conductive carbon clusters. Additionally, interfacial polarization, associated to a Maxwell-Wagner type of relaxation observed in heterogeneous materials, was supposed to contribute to the increase of AC conductivity [17]. The increase of carbonization temperature of wood charcoal induced an increase of the high frequency AC conductivity [15,18] up to the achievement of the percolation threshold, when a direct current (DC) conductivity was measured. In this regime of full percolation, the rise of intrinsic conductivity of the carbon clusters due to the healing of defects led to the increase of the DC conductivity [18–20]. The presence of defects such as pores and inorganic elements should be also taken into account to interpret correctly the temperature variations of the electrical conductivity [15,21].

Scarce literature is available on the influence of heating rate and feedstock composition directly on electrical conductivity, however since these two parameters are known to influence the chemical and physical characteristics of biochar [13], it is very likely that they also have an effect on its electrical properties.

More specifically, under the typical heating conditions of slow and fast pyrolysis differences in the biochar characteristics such as porosity and graphitization were observed due to heating rate variations [22]. At low temperature, when devolatilization is the prevailing phenomenon responsible of biochar porosity, higher heating rates accounted for the loss of surface area of biochar due to the rapid devolatilization destructing the biomass matrix and the occurrence of melting phenomena [23]. Conversely, at higher temperatures, under the thermal annealing regime, numerous authors [24–27] agree that higher heating rates provide higher surface areas due to the lower extent of volatiles repolymerization reactions responsible of sealing off the biochar micropores and to the lower order of graphite-like clusters in the carbon matrix.

Concerning biomass composition, it is known that organic components and inorganic elements evolve differently during the thermal treatment, the latter also catalyzing some conversion pathways of the organic matrix [28–30]. Biochars from cellulose, hemicellulose and lignin exhibited different chemical and structural characteristics. Indeed, the different volatiles content of the three components and melting phenomena observed for hemicellulose and lignin affected biochar porosity [31]. Moreover, cellulose and hemicellulose showed a higher tendency to lose oxygen and form polyaromatic graphite-like structure at high temperature [32]. Byrne and Nagle [33] postulated that a preferred orientation in the carbonized wood results from a preferred orientation of cellulose molecules in the secondary walls of longitudinal cells whereas carbon fibers obtained by lignin at 2000°C exhibited inhomogeneous graphitic structure probably catalyzed by inorganic impurities on a local level [34]. Differences in biomass composition resulted in different values of electrical conductivity ranging from 10^{-3} to 10^{4} S/m for biochar produced at different pyrolysis temperatures [35] reported values from 0.2 to 200 S/m for biochar obtained at 900°C from different lignins. However, it is difficult to identify the specific role of biomass composition given the different production temperatures and electrical conductivity measuring procedure.

In addition, the influence of different amounts of biochar used in composite preparations makes even more difficult to compare the electrical conductivity of composites prepared with biochars of different origins. At the same biochar/polymer ratio, higher electrical conductivity values were observed as biochar production temperature increases [6] whereas a non-monotonous trend was observed at increasing biochar percentage in the composite [36]. Also the biomass source produced different electrical conductivity in the corresponding composites mainly due to the different aromaticity of the produced biochars [36].

However, it is still unclear to what extent the chemical and structural differences induced by different heating rates or by the variability of feedstock composition may affect the electrical properties of biochar and final composites. This study aim at paving the way to shade light on this literature gap by studying the chemical and structural differences of biochars produced from three feedstock at different pyrolysis temperature in the range 500–700 °C under slow and fast pyrolysis conditions. Electrical conductivity in DC has been used as indicator of biochar ability to conduct current. The biochar were extensively characterized (Raman spectroscopy, field emission scanning electron microscopy (FESEM), Fourier-transform infrared spectroscopy (FT-IR), adsorption porosimetry) with the goal of finding possible correlations with their electrical conductivity and with the electrical conductivity of biochar-epoxy resin composites prepared with the best performing biochars.

2. Experimental

2.1. Feedstock

Three feedstocks were selected in this study for the production of biochars: namely sewage sludge (SS) from a municipal waste treatment plant, lignin rich residue (LRR) from an industrial bio-ethanol production site and walnut shells (WS) provided by Schicker Mineral. Feedstock preparation and characterization procedures are reported in Supplementary Material.

2.2. Biochar production and characterization

Three series of biochars were produced from SS, LRR and WS under slow and fast pyrolysis conditions at three temperatures, 500 °C, 600 °C and 700 °C in two different reactors described in the Supplementary Material. In case of SP biochar represents the primary product of the

process, whereas it represents a by-product in case of FP which is preferred to maximize liquid yield; however, its utilization is strongly recommended to increase the sustainability of liquid bio-fuel production. The lower limit of the temperature range was chosen taking into account that FP for liquid bio-fuel production is typically conducted at about 500°C. On the other hand, the upper temperature limit was fixed at 700 °C since SP temperature for biochar production should not achieve very high temperature to avoid excessive reduction of biochar yield. Moreover, a relevant change in biochar resistivity occurred between 500 and 700 °C [37] and the critical value observed in the literature for cellulose and wood reaching the percolation threshold falls within this temperature range [15,18].

All biochars were characterized for chemical and structural properties that were found to be relevant to determine the electrical conductivity of the biochar itself and biochar-based composites. Only for SS sample and the corresponding biochars, the composition of the inorganic fraction was analyzed by inductively coupled plasma-mass spectrometry (ICP/MS) according to the procedure reported in the Supplementary Material to assess the environmental risk associated to the possible heavy metals emission during pyrolysis.

Elemental analysis (see Supplementary Material) allows to calculate O/C and H/C ratios. O/C ratio is an indicator of the presence of polar functional groups, such as hydroxyl and carboxyl groups, contributing to the determination of the electrical conduction through the dipole polarization mechanism [15]. H/C ratio is typically considered a measure of the progress of the graphitization process characterized by the formation of carbon atoms with sp2 hybridized orbitals and electrons delocalized in a p orbital responsible of the electrons conduction.

FTIR spectra in the 3600–400 cm^{-1} range were also recorded to monitor the evolution of biochar polar and aromatic functionalities. The spectra were acquired in transmission mode on a Perkin-Elmer MIR spectrophotometer on pellets obtained upon compression of powdered dispersions prepared by mixing and grinding the samples (~1 wt.%) with KBr. The spectra were acquired with a resolution of 2 cm^{-1} by collecting 8 scans and correcting the background noise.

The study of evolution of Raman spectra as function of pyrolysis temperature provides important insights on the material structure. Raman spectra were recorded in the range from 250 cm^{-1} to 3500 cm^{-1} using a Renishaw inVia^{TM} (H43662 model, Gloucestershire, UK) equipped with a green laser line (514 nm) with a 50X objective. The characteristics D and G bands, ~1350 cm-1 and ~1580 cm-1, respectively, arise from sp2 coordinated regions. D peak is related to the presence of edges and grains while G peak arises from sp2 coordinated carbon atom pairs [38]. The ratio of the peak intensity of D-band to G-band also known as I_D/I_G together with the peak widths is used to assess the evolution from an amorphous carbonaceous structure to a graphitic structure in biochar [38].

Proximate analysis (see Supplementary Material) provides information on the ash content of the different biochars. Inorganic elements are typically detrimental to electrical conductivity and should be taken into account to explain some phenomena observed during electric conduction in carbonaceous materials [15,21].

The porosity of the biochars was characterized by gas adsorption porosimetry. The development of internal porosity can affect electrical conductivity of the biochar since pores act as defects in the formation of ordered graphite-like carbonaceous structure [15,21]. High resolution equilibrium nitrogen adsorption/desorption isotherms at -196°C were obtained in a volumetric analyzer (Quantachrome, Autosorb iQ). The samples were previously outgassed under vacuum at 200°C for 5 h. The Brunauer-Emmett-Teller (BET) theory was used to calculate the specific surface areas and total pore volumes were measured at $p/p^{\circ}=0.97$. Micropores and mesopores volume and surface were calculated applying the t-plot method and the Barrett-Joyner-Halenda (BJH) theory, respectively, whereas macropores volume was calculated as difference between total pore volume and micro- and meso- pores volume.

FESEM analyses were performed with a Zeiss SupraTM 40 to investigate the biochar morphology.

The experimental set-up for electrical conductivity measurements was adapted from Gabhi et al. [39]. It is composed of two solid copper cylinders, 30 mm in diameter and 5 cm in length, encapsulated in a hollow Plexiglas cylinder with a nominal inner diameter of 30 mm in the case of filler electrical characterization. In this configuration, the inner diameter is slightly higher so that it is possible to force the copper rods inside the Plexiglas cavity and the upper rod can slide inside the cylinder during the measurement. This arrangement creates an internal chamber between the two cylinders, where the biochar powder can be inserted. In case of composite the Plexiglas cylinder was removed and the sample was positioned between the aligned copper cylinders. The electrical resistance of the powders or composite was measured at increasing loads (up to 1400 bar) applied by a hydraulic press (Specac Atlas manual hydraulic press 15T). Electrically insulating sheets were placed between the conductive cylinders and the load surfaces in order to ensure that the electrical signal pass through the sample. The resistance of the biochar fillers was measured using an Agilent 34401A multimeter and used to calculate electrical conductivity according the following equation (Eq. (1)):

$$\sigma = 1/\varrho = l\cdot(R\cdot S)^{-1} \quad (1)$$

Where σ, S/m, is the electrical conductivity, ρ [$\Omega\cdot m$], is the electrical resistivity, l [m], R [Ω], and S [m^2], are the length, the electrical resistance and the surface of the specimen, respectively.

2.3. Composite preparation and characterization

Biochar based epoxy composites were produced using a two component bis-phenol A (BPA) diglycidyl resin (CORES epoxy resin, LPL) according to methodology developed by Bartoli et al. [40]. Carbonaceous fillers were dispersed into epoxy monomer using a tip ultrasonicator apparatus (Sonics Vibra-cell) for 15 min with on/off cycles of 20 and 10 s to avoid the temperature rising during the mixing. After the addition of the curing agent, the mixture was ultrasonicated for 2 min by using the same procedure. Biochar blends were put into silicon moulds for 16 h at room temperature. A final thermal curing was performed using a ventilated oven (I.S.C.O. Srl) at 70 °C for 6 h. Electrical conductivity measurements were performed using the same apparatus and procedure adopted for biochars (see Section 2.2).

3. Results

3.1. Feedstock characterization

The results of feedstock elemental and proximate analyses are reported in Table 1, whereas the metal ions content is reported in the Supplementary Material, Table S1. The values reported in Table 1 are the average of two replicates with a relative error lower than 5% of the measured value. It is important to specify that, while in the LRR and WS samples the balance of C, H, N and ash can be closed, with a good level of accuracy, with oxygen, in the SS sample the presence of other elements not belonging to the ash category, such as S and Cl, should be considered, whose content is not negligible although much lower than that of oxygen [41]. In Table 1 these elements will be referred to as 'others'.

The SS sample had the lowest carbon and oxygen content due to the high content of ash whose composition was dominated by the presence of metal ions such as P, Al, Fe, and Ca. These ions are mainly in form of phosphates (fertilizers, human and animal excrements), sulphates and lime (added during sludge flocculation stage in municipal wastewater treatment plants) [42]. Non negligible amounts of metal ions typically classified as trace metals [43] were also detected in SS ash. In this regard, the fate of toxic elements (e.g. heavy metals) during pyrolysis should be assessed to monitor the environmental risks associated to their emission.

Table 1
Elemental and proximate analysis of SS, LRR, WS and of derived biochars.

	C	H	N	O+others	Volatiles	Fixed Carbon	Ash
	wt%, daf basis				wt%, db		
SS	51.9	7.4	8.8	31.9	65.3	10.6	24.1
LRR	55.8	6.7	0.8	36.7	69.6	22.4	8
WS	50.2	6.4	0.1	43.2	79.7	20	0.3
SS 500 SP	57.4	2.5	9.4	30.8	40.8	11.5	47.7
SS 600 SP	78.8	1.3	9.2	10.7	27.5	20.1	52.4
SS 700 SP	80.3	1.2	11.6	6.8	26.2	22.1	51.7
SS 500 FP	74.0	3.1	10.9	12.0	30.5	10.9	58.6
SS 600 FP	76.4	1.1	9.6	12.8	26.6	9.3	64.1
SS 700 FP	80.1	1.0	8.5	10.4	22.6	10.6	66.8
LRR 500 SP	88.2	3.0	0.5	8.3	18.0	60.7	21.3
LRR 600 SP	89.7	2.2	0.5	7.6	14.1	63.7	22.2
LRR 700 SP	92.5	1.2	0.5	5.8	11.0	66.4	22.6
LRR 500 FP	64.8	2.6	0.8	31.8	21.5	50.2	28.3
LRR 600 FP	69.4	1.5	0.6	28.5	18.1	50.6	31.3
LRR 700 FP	70.2	1.0	0.6	28.2	17.1	53.2	29.7
WS 500 SP	80.2	3.2	0.1	16.5	28.9	70.1	1.0
WS 600 SP	85.1	2.3	0.1	12.5	22.5	76.4	1.1
WS 700 SP	88.3	1.9	0.1	9.8	17.9	80.9	1.2
WS 500 FP	68.8	4.7	0.1	26.4	45.0	53.8	1.2
WS 600 FP	76.9	3.7	0.1	19.3	33.8	65.0	1.2
WS 700 FP	87.4	2.1	0.1	10.5	19.3	79.5	1.2

The LRR carbon content was higher than the typical values observed for woody or herbaceous biomass [44] and responsible of the low oxygen content. This result is due to the removal of carbohydrates occurred during the pre-treatment stage of the bio-ethanol production process. However, it should be noted that the fixed carbon content of LRR was greatly lower than that measured for commercial alkali lignin [28], thus suggesting that a relevant fraction of non-ligninic material was still present in the LRR sample.

Compositional analysis confirmed this observation. Indeed, it shows that even though LRR has a high lignin content (52.6 wt% db), it contains also an unusual high amount of extractives (31.8 wt% db) and a very low amount of holecellulose (7.6 wt% db). Typically water and ethanol used in the NREL procedure extracts hydrophilic compounds such as polyphenols. However, since LRR is the residue of biomass undergone an acid pre-treatment, it is likely that most of the carbohydrates polymers accounting for the holocellulose fraction were degraded in smaller molecules soluble in polar solvents [45] K and Ca are the most abundant metal ions in the ash fraction.

WS was characterized by the lowest content of ash mainly composed of K and Ca based compounds. The carbon and fixed carbon contents were higher than the typical values observed for woody and herbaceous biomasses consistently with the high lignin content obtained from the compositional analysis of this vegetal residue (55.3 wt.% db). The extractive content of WS is 7.3 wt% and the holecellulose fraction accounts for the remaining 35.8 wt.% (db).

FT-IR spectra of SS, LRR and WS were shown in Fig. 1.

For the three materials, the signals were distributed in four main regions: a region between 3000 and 3800 cm^{-1} containing signals of exchangeable protons (from alcohol, phenol, amine, amide and carboxylic acid groups), a region between 2800 and 3000 cm^{-1} containing signals due to the stretching of aromatic and aliphatic C-H groups, a region between 1800 and 750 cm^{-1} containing overlapped signals of

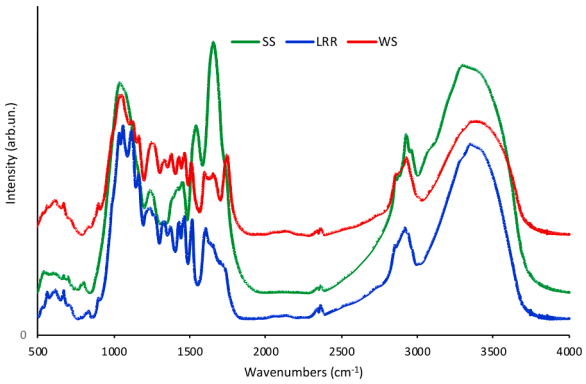

Fig. 1. FT-IR analysis. FT-IR spectra of SS, LRR, and WS.

stretching and bending absorptions of many different functional groups (C=O of carbonylic and carboxylic groups, C-OH, C-H, C=C, C-C), and a region below 700 cm^{-1} representing C–C stretching.

All the spectra exhibited a broad band at 3400–3500 cm^{-1} due to the hydroxyl groups in phenolic and aliphatic structures. In LRR and WS spectra the bands around 2940 and 2850 cm^{-1} are due to the CH stretching in aromatic methoxyl groups and in methyl and methylene groups of side chains in lignin structures [46] and hydrocarbon in polysaccharides [47]. In the SS spectrum these absorption bands are attributed to aliphatic methylene groups and assigned to fats and lipids which represent an important fraction of sludges.

Noticeable differences were found between SS and the lignocellulosic materials in the region between 1800 and 750 cm^{-1}, whereas WS and LRR spectra were more similar, at least from the qualitative point of view. Two broad bands centered at 1550, 1667 cm^{-1} were identified in SS spectrum and assigned to proteins, Amide II and Amide I, respectively [48]. In the same region, both LRR and WS exhibited signals of unconjugated or conjugated carbonyl/carboxy stretching, the unconjugated one being almost absent in WS sample [49]. In the region between 1600 and 1400 cm^{-1} peaks representing aromatic skeleton vibrations and aliphatic C–H deformations typical of lignin structure [49] were detected in both LRR and WS samples although the intensity of the bands may differ. The spectral region below 1400 cm^{-1} contained many overlapped peaks. Worth to be noted were the bands near 1130 cm^{-1}, 1170 cm^{-1} assigned to the symmetric and asymmetric C–O–C stretching of β-(1→4)-glycosidic linkages which are more intense in the WS and LRR samples and absent in SS. The presence of these bands in LRR sample confirmed the presence of a relevant fraction of residual carbohydrates.

Finally, in WS sample the peaks at 1080–1030 cm^{-1} corresponding to the unique broad band around 1550 in both LRR and SS spectra can be assigned to C–O stretching of polysaccharides or polysaccharide-like substances. In case of SS Si–O of silicate impurities, and clay minerals possibly in a complex with humic acid can contribute to increase the intensity of this peak [48].

The thermal behavior of SS, LRR and WS in N_2 was studied by termogravimetry following the evolution of the weight loss curves (TG) and their derivatives (DTG) as function of temperature shown in Fig. 2, panels a and b.

LRR devolatilization began at about 150°C as it occurs also for commercial alkali lignin [31]. However, whereas the devolatilization of alkali lignin proceeds gradually and is represented by a smooth, broad peak in the DTG curve, LRR was subjected to an abrupt weight loss in the range 280-340°C represented by a narrow peak in the DTG curve typically attributed to cellulose decomposition. In addition, a shoulder, typically attributed to devolatilization of hemicellulose, was faintly visible on the increasing branch of the DTG curve. At temperature higher than 340°C the devolatilization proceeded slowly up to 500°C and was almost complete. The evolution of LRR TG curve confirmed the presence of carbohydrates from the holocellulosic component of the parent

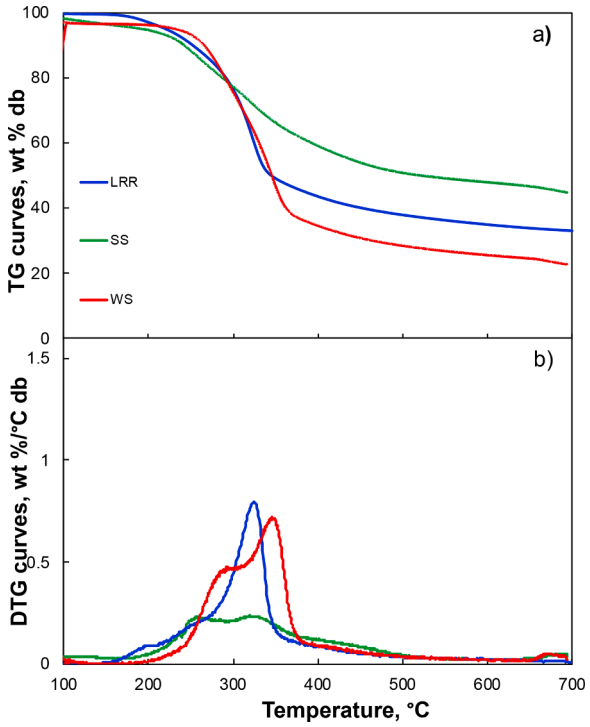

Fig. 2. Feedstock TG analysis. (a) TG and (b) DTG curves of SS, LRR and WS obtained in N_2 at 10°C/min.

feedstock, mainly from cellulose. The high yield of the solid residue at 700°C was due to the high lignin and ash content as shown from the compositional and proximate analyses, respectively.

WS devolatilization began at about 200°C and the two peaks of hemicellulose and cellulose decomposition were more pronounced and shifted to higher temperatures than observed for LRR, likely because of the very low content of alkali and earth alkali metals [50].

SS thermal decomposition evolved through two main overlapping peaks in the temperature range between 200 and 500°C where most of the weight loss occurred. The high ash content of the starting material contributes to the high solid residue at 700°C.

3.2. Biochar characterization

In the following, the different biochars will be referred to by acronyms defined as follows: feedstock acronym (SS, LRR and WS), temperature at which the biochar sample was produced (500, 600 and 700°C) and process acronym, namely SP and FP for slow and fast pyrolysis, respectively. Results of elemental and proximate analysis are reported in Table 1 as the average of two replicates with a relative error lower than 5% of the measured value. The progress of devolatilization as the pyrolysis temperature increased, led to a decrease in the volatile content and, conversely, an increase in the fixed carbon and ash content, except for SS derived biochars produced under FP conditions whose fixed carbon content remained almost unchanged as temperature increases. Except for the chloride salts, most of the inorganics in the biomass are typically retained up to very high temperature so that their concentration in the biochars is mainly determined by the extent of the organic matter devolatilization [51]. According to TG analyses, for all the three feedstocks only a mild devolatilization occur between 500 and 700°C, thus resulting in small variations of the ash content in this temperature range.

Results from proximate analysis of biochars form SP series were consistent with the initial composition of the initial biomass. LRR and WS biochars were characterized by higher fixed carbon content due to the presence of high amounts of lignin in the raw biomass samples. These biochars showed comparable volatiles and fixed carbon content, if compared on a daf basis. However, LRR derived biochars were characterized by higher ash content in agreement with LRR composition. SS derived biochars had the highest volatile content and the lowest fixed carbon despite the lower volatile content of SS. It can be argued that, differently from LRR and WS, SS devolatilization proceed substantially even at temperature above 700°C. Consistently with the SS composition, about half of the biochar samples were composed of ash. As regards ash composition,t is worth to be noted that all the heavy metals were completely retained in the biochars, except for Cd whose retention was reduced by about half at 500°C. Even though its initial concentration was very low in the SS sample used in this study, its release must be monitored during the thermal treatment and, where necessary, measurements should be considered to prevent its release into the environment.

The heating rate greatly affected the characteristics of biochars differently depending on the biomass considered. FP conditions promoted devolatilization reactions for all the feedstocks thus resulting in higher biomass conversion and increased ash content in the produced biochars. Lignocellulosic biomass, namely LRR and WS, under FP conditions produced biochars with higher volatile content and lower fixed carbon content. Tentatively, this result can be attributed to the longer residence time of the solid matrix at low temperature promoting cross-linking reactions during SP compared to FP. Under FP the conditions SS produced biochars with lower contents of both volatiles and fixed carbon, probably due to the high ash content and the different chemical nature of the starting material.

The biochars obtained from all three feedstocks exhibited an increase in carbon content at the expense of oxygen and hydrogen content as temperature increased, regardless the different heating rates.

The effect of feedstock and of the heating rate on the biochars chemical properties are compared through the Van Krevelen diagram in Fig. 3. O/C and H/C ratios decreased accordingly to the progress of the devolatilization of oxygenated compounds and the charring reactions.

The three feedstocks were characterized by very different O/C ratio, which was highest for WS, followed by LRR and SS. Under SP conditions, biochars from lignocellulosic feedstocks behaved similarly to the parent material in terms of O/C and H/C ratios in the whole temperature range, more specifically WS biochars have always higher O/C and H/C ratios than the corresponding LRR biochars. On the contrary, O/C and H/C ratios in SS biochars did not reflect the lowest O/C and highest H/C values observed in the parent material.

At 500°C WS and LRR lost a substantial fraction of oxygenated organic compounds, whereas their devolatilization was very limited for SS. This is consistent with the high content of volatiles still present in SS 500 SP. At 600°C SS showed a substantial decrease of O/C ratio and SS 600 SP was characterized by the lowest O/C ratio, followed by WS 600 SP and LRR 600 SP. It is worth to be noted that SS typically contains a relevant fraction of O bound to inorganic compounds in form of

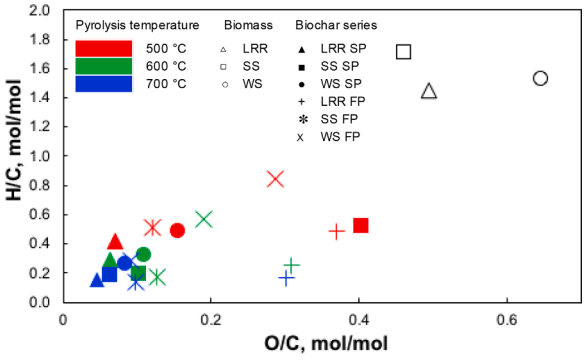

Fig. 3. Van Krevelen diagram. H/C vs O/C molar ratios for SS, LRR and WS (open symbols), SP (closed symbols) and FP (thin symbols) biochar series.

sulphates and phosphates that undergo thermal decomposition between 500 and 600°C [42,52], thus contributing to the reduction of the O/C ratio in this temperature range.

At 700°C O/C ratios of all the biochars fell within a narrow range between 0.05 and 0.08.

A drastic reduction of H/C ratio was observed in the biochars produced at 500°C, reaching similar values regardless of the type of feedstock. At higher temperature WS derived biochars had always higher H/C ratios than LRR and SS derived biochars.

Large differences were observed in biochars obtained under slow and fast pyrolysis conditions. Higher O/C and H/C content were measured for both LRR FP and WS FP biochars with respect to the corresponding biochars of SP series. However, differently from biochars from SP series, FP biochars did not reflect the relative O/C and H/C values of the parent materials. Consistently with the results of proximate analysis, at 500°C SS underwent an enhanced devolatilization under FP conditions resulting in lower O/C ratio of SS 500 FP. On the contrary, H/C values were not affected by heating conditions.

Raman spectra of all the biochars are shown in Fig. 4. Two main peaks were identified, the G peak, located in the 1550-1615 cm^{-1} range, and the D peak centred at 1250 cm^{-1}. A second order region of overlapped peaks (G', D+G, 2G, 2D') also appeared from 2250 to 3500 cm^{-1}.

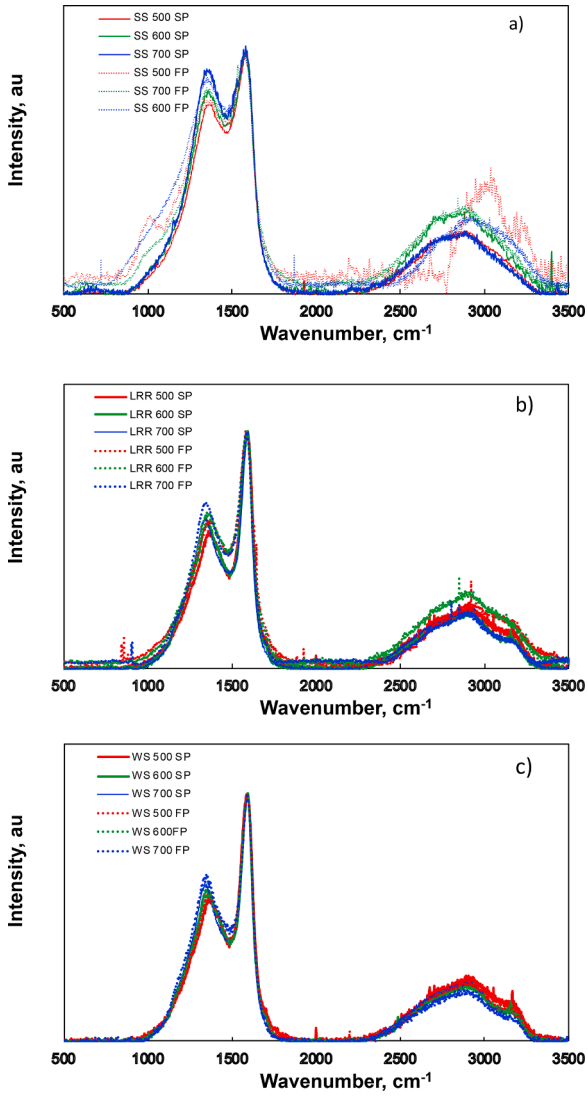

Fig. 4. Biochars Raman spectra. Raman intensity as function of shift of (a) SS, (b) LRR, and (c) WS derived biochars obtained at 500, 600 and 700°C under SP and FP conditions.

Each spectrum was normalized on the G peak to compare the different biochars. For each biochar series D peak increased with the pyrolysis temperature. The D peak was very pronounced in SS derived biochars, whereas for the biochars of LRR series it was only slightly higher than for the WS derived biochars. According to the three-stage phenomenological model proposed by [38], it can be postulated that all the biochars are into the second stage of the amorphization trajectory where an initial transition from amorphous carbon to nanocrystalline graphite occurs. In this stage the Tuinstra and Koenig equation is no longer valid [53] and the relative intensity of D to G peak is not inversely correlated to the average size of crystalline sp2 carbon clusters, but to the number of sp2 carbon in six fold rings. Therefore, the more pronounced D peak as pyrolysis temperature increases denoted an increasing number of six fold condensed aromatic rings with defects still far from being structured in ordered graphitic clusters. This result is consistent with the decreasing H/C ratio observed in biochars produced at increasing temperature. The aromatic character of the biochars is more pronounced in SS SP biochars despite the high lignin content of LRR and WS, since most of the N-containing species present in SS evolve to aromatic compounds during pyrolysis [54]. In SS derived biochars, and to a less extent in LRR biochars, the massive presence of inorganics enhanced the defects in carbon structures.

There are not remarkable differences between the WS and LRR and SS derived biochars in dependence on the pyrolysis heating rate suggesting that fast and slow pyrolysis of these biomasses follow similar fundamental chemistry processes [55]. Worth to be noted is that fast heating rate promoted the presence of peaks at low wavenumbers and a pronounced shoulder on the D peak reasonably due to oxides species consistently with the higher ash content of SS FP biochars with respect to SS SP ones . Considering the high content of iron and other metals, the submicrometric particles could be formed during pyrolytic conversion through carbothermal process as reported in the literature for iron oxides [56] and nitrates [57].

Fig. 5 shows several SEM micrographs of all the biochars produced at 700°C at different levels of magnification. The most meaningful observation that can be deduced from the images is related to LRR biochars. More specifically, structural transformations of LRR under FP were observed with evident signs of melting and development of macropores. The propensity of biochar to melt under the fast heating conditions was previously observed for other biomass types and the primary role played by lignin in the formation of metaplast was established [58]. Moreover, it was previously documented that potassium and calcium bahave as active catalysts in the metaplast formation [59]. Indeed, LRR, differently from SS and WS, is characterized by the concomitant presence of high amounts of lignin, potassium and calcium.

Residual functionalities on the biochar surfaces were detect by using FT-IR spectroscopy as shown in Fig. 6.

All samples produced at 500°C under SP conditions showed a $\nu_{C=C}$ band at around 1600 cm^{-1} due to the presence of aromatic rings. SS 500 SP and WS 500 SP showed a broad ν_{O-H} band from 3000 cm^{-1} up to around 3500 cm^{-1} due to residual hydroxyl groups. LRR 500 SP showed also bands in the range from 1700 cm^{-1} up to 2000 cm^{-1} suggesting the presence of carboxylic functionalities of LRR. SS 500 SP spectrum displayed an intense band peaked at around 1013 cm^{-1} that become weaker in SS 600 SP, reasonably due to the overlapping of several vibration modes such as ν_{C-O}, δ_{C-O} and $\nu_{Si-O-Si}$ [40]. By increasing the pyrolysis temperature up to 600°C, LRR and WS derived biochars did not show any appreciable evolution of IR spectra but SS derived biochar showed a considerable simplification. Indeed, only an intense peak due to $\nu_{C=C}$ of aromatic rings at around 1600 cm^{-1} and few other bands mainly due to ν_{C-O}, δ_{C-O} were detected suggesting the occurrence of the aromatization process of the carbonaceous matrix. By increasing the pyrolysis temperature up to 700°C, the cracking reactions induced by the inorganic component of SS promoted the degradation of the organic matters. Accordingly, the resulting spectrum was characterized by the $\nu_{Si-O-Si}$ band as major component. Both LRR 700 and WS 700 SP showed

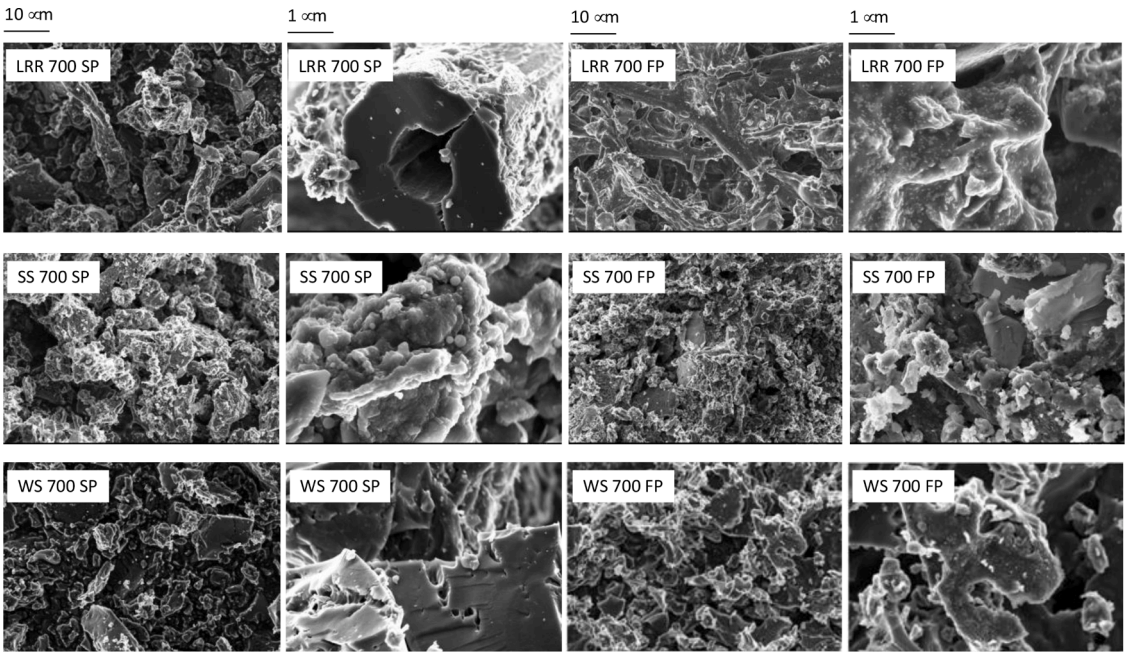

Fig. 5. Biochars FESEM images. FESEM micrographs at different magnifications of biochars produced at 700°C under FP and SP.

a simplification of the spectra testifying the massively loss of surface functional groups. All the biochars of FP series produced at 500°C did not exhibit relevant differences with the corresponding biochars of SP series. However, as temperature increased, differently from biochars of SP series, they showed similar spectra and the intensity of the peaks was only slightly attenuated even in biochars produced at 700°C, except for WS 700 FP which displayed a spectrum with relevant band at 1063 cm^{-1} and 1118 cm^{-1} due to $\nu_{C\text{-}O}$ and $\delta_{C\text{-}O}$. This is reasonably due to the massively presence of oxygen based functionalities such as ethers and hydroxyl groups formed due to the faster heating rate. Only $\nu_{O\text{-}H}$ band from 3000 cm^{-1} up to around 3500 cm^{-1} disappeared at high temperature similarly to biochars of SP series.

The evolution of the BET surface and of the pore volume of the biochars from the different feedstocks at increasing temperature is reported in Table 2. Under slow pyrolysis conditions, as the temperature increased, the progress of the devolatilization reactions determined the increase of total pore volume, micropores volume and BET surface. In presence of high content of inorganics sintering phenomena can occur due to the formation of low melting point salts. Fused intermediates are detrimental for the development of the internal porosity by blocking the access to the pores. Consistently, higher BET surface with a well-developed microporosity were observed for WS derived biochars. Despite the high inorganic content of the LRR derived biochars, BET surface and total pore volume were greatly higher than the ones measured in SS derived biochars. As evidenced by Fig. 5, LRR during SP partially preserved its original structure due to the presence cellulosic fibers typically characterized by high porosity [31]. The presence of a large-scale texture made of a macro-porous cortical region and a core region characterized by large voids has been reported also for experiments of LRR pyrolysis and torrefaction in fluidized bed [60–62]. In contrast, SS, besides the high inorganics content, was an extremely deconstructed material due to the treatment process it went through.

Heating rate affected biochar porosity in terms of both BET surface and pore volume differently depending on the pyrolysis temperature and feedstock. More specifically, BET surface and pore volume of LRR biochars produced under FP conditions are greatly lower than the corresponding biochars of SP series, whereas porosity of SS and WS biochars seems to be scarcely affected by heating rate variations. This is consistent with the evident sing of melting observed in SEM micrographs of LRR biochars reported in Fig. 5.

It is worth to be noted that WS biochars produced under fast pyrolysis conditions exhibited a non-monotonous trend with the temperature. WS 500 FP and WS 600 FP had a higher BET surface and total pore volume than the corresponding biochars obtained in slow pyrolysis experiments. This can be explained considering that during fast pyrolysis a disruptive volatilization and a rapid shrinking of the solid phase occurred that altered the structure of the biomass causing the coalescence of micropores and the formation of larger pores and cracks inside the solid matrix. While creating larger pores from the coalescence of micropores would reduce the internal surface area, a more open structure offers less resistance to mass transfer through the pores, thus reducing the partial occlusion of the micropores due to the volatiles repolymerization reactions. At 700°C the negative effect of micropores coalescence on the biochar internal surface prevailed and the BET surface decreased becoming even lower than the one of WS 700 SP.

The different chemical and structural properties of the biochars greatly affected their electrical conductivity.

As clearly emerged from Fig. 7, all the biochars produced at 500°C showed very low conductivity along all the investigated pressure range. This was essentially due to the poor graphitization occurring at this temperature consistently with the high H/C values and the low intensity of the D peak in the Raman spectra. As temperature increased up to 600°C a considerable improvement of conductivity was observed for all the biochars. At 600°C, the decrease of O/C and H/C ratio and the increase of the intensity of the D peak in the Raman spectra denoted an increase of carbon atoms with sp2 hybridization into polycondensed clusters of six fold rings. The percolation model suggests that the increase of conductivity could be due to the reduced distance between conductive carbon clusters that became short enough to allow electron hopping. At 700°C a further increase of the conductivity of about three orders of magnitude was observed for all the biochars thus suggesting the achievement of the percolation threshold and the formation of a highly conductive carbon region. Biochars produced at 500 and 600°C from different feedstocks exhibited different conductivity, whereas those produced at 700°C had comparable electrical conductivity regardless their origin. Results obtained in the present study for biochars produced at 700°C, were in good agreement with the ones observed for biochars produced at similar temperatures under slow pyrolysis

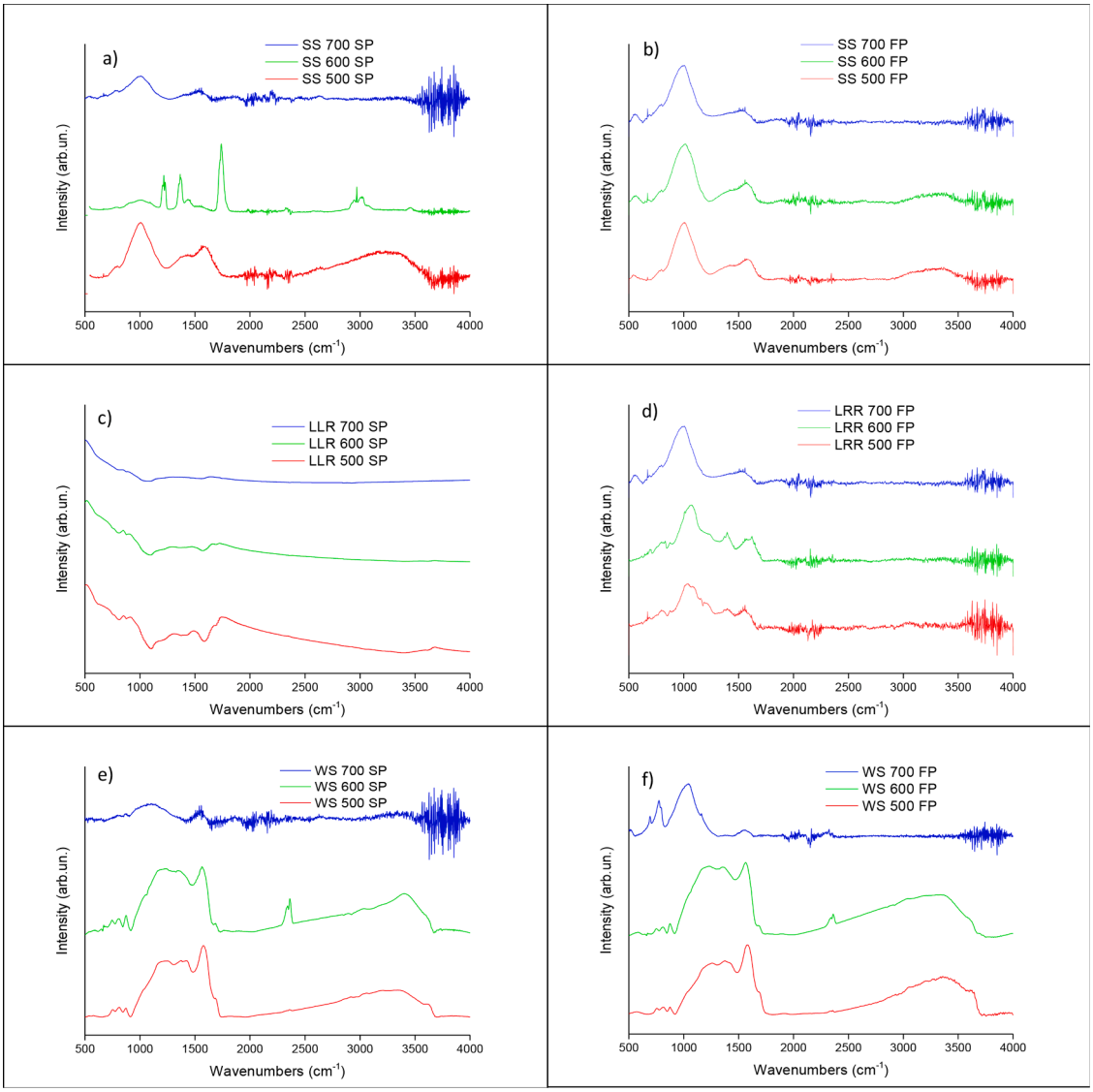

Fig. 6. FT-IR analysis. FT-IR spectra of (a) SS SP, (b) SS FP (c) LRR SP, (d) LRR FP, (e) WS SP and (f) WS FP biochars obtained at 500, 600 and 700°C.

Table 2
Porosity analysis of SS, LRR, WS derived biochars.

Sample	BET, m^2/g		Tot pore volume, cm^3/g		Micropore volume, cm^3/g	
	SP	FP	SP	FP	SP	FP
SS 500	5.6	7.8	0.0136	0.0313	0.0010	$<10^{-4}$
SS 600	5.5	8.5	0.0151	0.0387	0.0009	$<10^{-4}$
SS 700	8.4	10.2	0.0151	0.0413	0.0020	$<10^{-4}$
LRR 500	45.2	10.6	0.0560	0.0202	0.0020	0.0010
LRR 600	251.0	16.1	0.1468	0.0327	0.0860	$<10^{-4}$
LRR 700	315.8	14.3	0.1591	0.0288	0.1020	0.0010
WS 500	26.8	32.9	0.0254	0.0404	$<10^{-4}$	$<10^{-4}$
WS 600	319.1	370.7	0.1487	0.1899	0.1160	0.1240
WS 700	365.6	296.2	0.1520	0.1540	0.1150	0.0970

conditions ranging between 10^{-2} and 1 S/m [35]; however, the electrical conductivity of commercial carbon black is significantly higher.

Concerning the effect of feedstock it can be observed that at 500 and 600 °C under slow pyrolysis conditions, SS derived biochars had higher conductivity compared to the biochars obtained at the same temperatures and heating rate from LRR and WS. Several mechanisms can be invoked to clarify this result. The higher intensity of the D peak in the Raman spectra of SS derived biochars denoted a higher number of six fold condensed aromatic rings even though still far from being structured in ordered graphitic clusters. Moreover, the higher volatile content of these biochars together with high O/C ratios suggest that at these temperatures biochars are still rich in polar oxygenated functional groups contributing to the conduction process as supported also by the analysis of the IR spectra. Finally, considering that most of the inorganics in SS were in form of salts it is likely that also interfacial polarization affected positively the conductivity of SS 500 SP and SS 600 SP.

Except for the porosity and ash content, the differences between the biochars chemical properties decreased as the temperature increased, and this explains the slight differences in electrical conductivity observed in the biochars produced at 700°C.

Comparing the biochars of SP and FP series, it appears that the higher heating rate positively affects the electrical conductivity of biochars produced at 500 and 600 °C, although to a lesser extent than the pyrolysis temperature. Different explanations can be given for biochars depending on the different feedstocks. LRR biochars from FP series were characterized by higher intensity of D peak with respect to the corresponding biochars of SP series. Moreover, biochars of FP series produced at 500 and 600°C had higher O/C ratios and more intense signals of oxygen-based functionalities denoting a higher concentration of polar

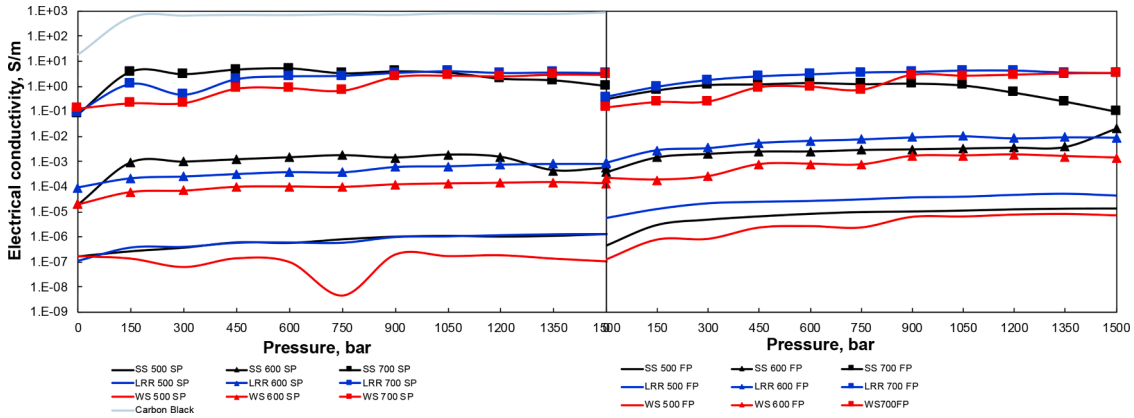

Fig. 7. Electrical conductivity of biochars and commercial carbon black (VULCAN® 9 N115) as a function of pressure.

oxygenated functional groups. Both these characteristics contributed to increase electrical conductivity of biochars from FP series. In case of WS derived biochars, given the similar Raman spectra denoting comparable graphitization level, only the higher content of polar oxygened functionalities can be invoked to explain the higher electrical conductivity of biochars of FP series. Finally, for SS biochars of FP series the higher electrical conductivity could be ascribed to the higher content of ash in form of salts responsible of an increased interfacial polarization.

3.3. Composites electrical conductivity

The electrical conductivity of composites prepared with biochars produced at 700°C under SP and FP conditions are shown in Fig. 8. Despite the comparable electrical conductivity of these biochars, their different origin affected the electrical properties of the corresponding composites.

Among the biochars of SP series, LRR 700 SP produced a composite with the highest conductivity reaching a value of about 0.02 S/m that was one order of magnitude higher compared to that of the composites containing WS 700 SP. SS 700 SP biochar did not lend any electrical conducting property to the corresponding composite.

It can be postulated that differences in particle size distribution affected the dispersion of the filler in the resin matrix. Indeed biochars, given their different volatiles and ash content, and porosity, could be characterized by different grindability [63,64] thus producing a different particle size distribution after the grinding stage of the composite preparation procedure. This speculation was supported by FESEM analysis of grinded biochars (Fig. 5) that showed that coarser particles were obtained for SS 700 SP and it is consistent with the high ash and volatile content and low porosity of this biochar [64]. In the SS 700 SP based composite coarser particles could form aggregates separated by a thick polymer layer acting as an insulating barrier, thus preventing the achievement of the percolation threshold [65]. FESEM micrographs were not suitable to detect differences in the particle size distributions of the other biochar samples. According to its lower volatile content, LRR 700 SP should be more grindable than WS 700 SP [64], but its high ash content would drive in the opposite direction. The effect of the porosity is not clear since, even though the total pore volume of LRR 700 SP is higher than that of both WS 700 SP, LRR 700 SP was characterized by a lower macropores volume (0.0091 cm^3/g) than that of both WS 700 SP (0.015 and 0.046 cm^3/g, respectively). It can be postulated that the pore volume distribution among micro-, meso- and macro- pores could affect the biochar grindability with macropores playing a predominant role.

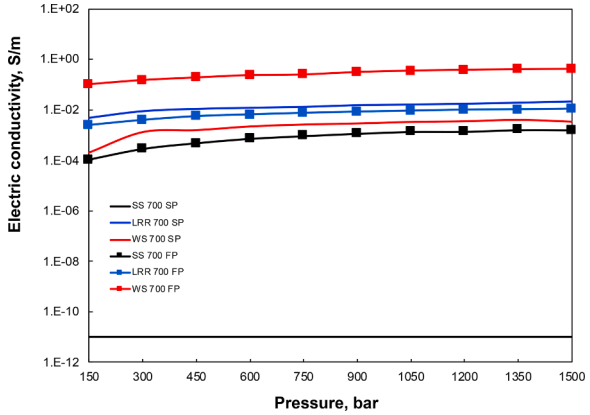

Fig. 8. Composites electrical conductivity. Electrical conductivity as a function of pressure of composites prepared with 40 wt% of biochars produced at 700 °C under SP and FP conditions.

Faster heating rate during biochars preparation affected positively the electrical conductivity of composites prepared with WS and SS derived biochars, whereas any relevant effect was observed on the electrical conductivity of LRR biochar based composites. Given the comparable values of the electrical conductivity of all the biochars used as fillers, it can be speculated that the observed differences were due to the different grindability affecting the dispersion of biochars particles into the resin. SEM micrographs showed finer particles in the SS 700 FP sample than in the SS700 SP biochar, while images of the WS 700 and LRR 700 samples were not suitable to give any indication of the difference in particle size. A dedicated work is needed in the future to clarify this aspect.

Finally, considering the residual functional groups detected through FT-IR spectroscopy, it is reasonable to assume that FP biochars could interact not only through π−π stacking interaction with aromatic moieties of the resin but also with polar residual functional groups [66]. This additional interaction boosted up the conductivity promoting a more efficient interaction of the filler network and a more homogenous dispersion.

4. Conclusions

The results reported in the present study showed that as the pyrolysis temperature is increased from 500 to 700°C, the electrical conductivity of biochars increases by about seven orders of magnitude, while the heating rate and the type of biomass have only a slight influence on the determination of electrical conductivity, especially at high temperature, despite the observed differences in the chemical and structural characteristics of biochars.

At lower temperatures (500 and 600°C) under slow pyrolysis conditions, SS derived biochars had higher conductivity compared to the biochars obtained at the same temperatures and heating rate from LRR and WS. The higher number of six fold condensed aromatic rings, the higher O/C ratio indicating the presence of O in polar oxygenated

functional groups and the higher content of inorganics in form of salts could affect positively to the electrical conductivity of SS 500 SP and SS 600 SP. At the same pyrolysis temperatures, fast heating led to a higher presence of polar oxygenated species resulting in a higher electrical conductivity. Biochars produced at 700°C under both slow and fast heating rate showed comparable electrical conductivity despite the differences in ash content and porosity.

There are indications that both the parent material and production heating rate of biochars influenced the electrical properties of the corresponding composites probably due to their influence on the grindability and surface chemistry affecting the interactions between biochar particles and epoxy resin. However, this analysis needs to be corroborated by further investigation.

CRediT authorship contribution statement

Mattia Bartoli: Investigation, Formal analysis, Writing – review & editing. **Maurizio Troiano:** Investigation, Formal analysis, Writing – review & editing. **Paola Giudicianni:** Conceptualization, Investigation, Formal analysis, Writing – original draft, Writing – review & editing. **Davide Amato:** Investigation, Visualization. **Mauro Giorcelli:** Supervision, Conceptualization, Writing – review & editing. **Roberto Solimene:** Supervision, Writing – review & editing. **Alberto Tagliaferro:** Supervision, Conceptualization.

Declaration of Competing Interest

The authors declare that they have no known competing financial interests or personal relationships that could have appeared to influence the work reported in this paper.

Acknowledgments

This research did not receive any specific grant from funding agencies in the public, commercial, or not-for-profit sectors .The authors wish to thank Massimo Rovere for her help with Raman characterization and Salvatore Guastella for FESEM characterization.

Supplementary materials

Supplementary material associated with this article can be found, in the online version, at doi:10.1016/j.jaecs.2022.100089.

References

[1] Antoniou N, Zabaniotou A. Re-designing a viable ELTs depolymerization in circular economy: pyrolysis prototype demonstration at TRL 7, with energy optimization and carbonaceous materials production. J Clean Prod 2018;174:74–86. https://doi.org/10.1016/J.JCLEPRO.2017.10.319.
[2] Brown TR, Wright MM, Brown RC. Estimating profitability of two biochar production scenarios: slow pyrolysis vs fast pyrolysis. Biofuels Bioprod Biorefining 2011;5:54–68. https://doi.org/10.1002/BBB.254.
[3] Bartoli M, Giorcelli M, Jagdale P, Rovere M, Tagliaferro A. A review of non-soil biochar applications. Mater 2020;13:261. https://doi.org/10.3390/MA13020261. 2020, Vol 13, Page 261.
[4] Das O, Bhattacharyya D, Sarmah AK. Sustainable eco–composites obtained from waste derived biochar: a consideration in performance properties, production costs, and environmental impact. J Clean Prod 2016;129:159–68. https://doi.org/10.1016/J.JCLEPRO.2016.04.088.
[5] Noori A, Bartoli M, Frache A, Piatti E, Giorcelli M, Tagliaferro A. Development of pressure-responsive polypropylene and biochar-based materials. Micromachines 2020;11:339. https://doi.org/10.3390/MI11040339.
[6] Giorcelli M, Bartoli M. Development of coffee biochar filler for the production of electrical conductive reinforced plastic. Polym 2019;11:1916. https://doi.org/10.3390/POLYM11121916.
[7] Torsello D, Ghigo G, Giorcelli M, Bartoli M, Rovere M, Tagliaferro A. Tuning the microwave electromagnetic properties of biochar-based composites by annealing. Carbon Trends 2021;4:100062. https://doi.org/10.1016/J.CARTRE.2021.100062.
[8] Torsello D, Bartoli M, Giorcelli M, Rovere M, Arrigo R, Malucelli G, et al. High frequency electromagnetic shielding by biochar-based composites. Nanomater 2021;11:2383. https://doi.org/10.3390/NANO11092383.
[9] Ziegler D, Palmero P, Giorcelli M, Tagliaferro A, Tulliani JM. Biochars as innovative humidity sensing materials. Chemosens 2017;5:35. https://doi.org/10.3390/CHEMOSENSORS5040035. 2017, Vol 5, Page 35.
[10] Spahr M.E., Gilardi R., Bonacchi D. Carbon black for electrically conductive polymer applications 2017:375–400. 10.1007/978-3-319-28117-9_32.
[11] Tang W, Santare MH, Advani SG. Melt processing and mechanical property characterization of multi-walled carbon nanotube/high density polyethylene (MWNT/HDPE) composite films. Carbon N Y 2003;41:2779–85. https://doi.org/10.1016/S0008-6223(03)00387-7.
[12] Hung MT, Choi O, Ju YS, Hahn HT. Heat conduction in graphite-nanoplatelet-reinforced polymer nanocomposites. Appl Phys Lett 2006;89:023117. https://doi.org/10.1063/1.2221874.
[13] Giudicianni P, Ragucci R. Chapter 2 controlling the conversion of biomass to biochar. 2020. https://doi.org/10.1088/978-0-7503-2660-5ch2.
[14] Kercher AK, Nagle DC. Microstructural evolution during charcoal carbonization by X-ray diffraction analysis. Carbon N Y 2003;41:15–27. https://doi.org/10.1016/S0008-6223(02)00261-0.
[15] Rhim YR, Zhang D, Fairbrother DH, Wepasnick KA, Livi KJ, Bodnar RJ, et al. Changes in electrical and microstructural properties of microcrystalline cellulose as function of carbonization temperature. Carbon N Y 2010;48:1012–24. https://doi.org/10.1016/J.CARBON.2009.11.020.
[16] McLachlan DS, Cai K, Sauti G. AC and dc conductivity-based microstructural characterization. Int J Refract Met Hard Mater 2001;19:437–45. https://doi.org/10.1016/S0263-4368(01)00024-5.
[17] Sugimoto H, Norimoto M. Dielectric relaxation due to the heterogeneous structure of wood charcoal. J Wood Sci 2005;51:554–8. https://doi.org/10.1007/S10086-005-0705-Z. 2005 516.
[18] Kercher A.K., Nagle D.C. Letters to the Editor AC electrical measurements support microstructure model for carbonization: a comment on ÔDielectric relaxation due to interfacial polarization for heat-treated wood' n.d. 10.1016/j.carbon.2003.10.037.
[19] Giorcelli M, Savi P, Khan A, Tagliaferro A. Analysis of biochar with different pyrolysis temperatures used as filler in epoxy resin composites. Biomass Bioenergy 2019;122:466–71. https://doi.org/10.1016/J.BIOMBIOE.2019.01.007.
[20] Savi P, Yasir M, Bartoli M, Giorcelli M, Longo M. Electrical and microwave characterization of thermal annealed sewage sludge derived biochar composites. Appl Sci 2020;10:1334. https://doi.org/10.3390/APP10041334.
[21] Emmerich FG, de Sousa JC, Torriani IL, Luengo CA. Applications of a granular model and percolation theory to the electrical resistivity of heat treated endocarp of babassu nut. Carbon N Y 1987;25:417–24. https://doi.org/10.1016/0008-6223(87)90013-3.
[22] Mohanty P, Nanda S, Pant KK, Naik S, Kozinski JA, Dalai AK. Evaluation of the physiochemical development of biochars obtained from pyrolysis of wheat straw, timothy grass and pinewood: effects of heating rate. J Anal Appl Pyrolysis 2013;104:485–93. https://doi.org/10.1016/J.JAAP.2013.05.022.
[23] Cetin E, Gupta R, Moghtaderi B. Effect of pyrolysis pressure and heating rate on radiata pine char structure and apparent gasification reactivity. Fuel 2005;84:1328–34. https://doi.org/10.1016/J.FUEL.2004.07.016.
[24] Kumar M, Gupta RC. Influence of carbonization conditions on the gasification of acacia and eucalyptus wood chars by carbon dioxide. Fuel 1994;73:1922–5. https://doi.org/10.1016/0016-2361(94)90223-2.
[25] Guerrero M, Ruiz MP, Alzueta MU, Bilbao R, Millera A. Pyrolysis of eucalyptus at different heating rates: studies of char characterization and oxidative reactivity. J Anal Appl Pyrolysis 2005;74:307–14. https://doi.org/10.1016/J.JAAP.2004.12.008.
[26] Mermoud F, Salvador S, Van de Steene L, Golfier F. Influence of the pyrolysis heating rate on the steam gasification rate of large wood char particles. Fuel 2006;85:1473–82. https://doi.org/10.1016/J.FUEL.2005.12.004.
[27] †,‡*,‡†‡ Haiping Y, Rong Y, Hanping C, Chuguang Z, Dong Ho L, Liang DT. In-depth investigation of biomass pyrolysis based on three major components: hemicellulose, cellulose and lignin. Energy Fuels 2005;20:388–93. https://doi.org/10.1021/EF0580117.
[28] Ferreiro AI, Giudicianni P, Grottola CM, Rabaçal M, Costa M, Ragucci R. Unresolved issues on the kinetic modeling of pyrolysis of woody and nonwoody biomass fuels. Energy Fuels 2017;31:4035–44. https://doi.org/10.1021/ACS.ENERGYFUELS.6B03445.
[29] Ferreiro AI, Rabaçal M, Costa M, Giudicianni P, Grottola CM, Ragucci R. Modeling the impact of the presence of KCl on the slow pyrolysis of cellulose. Fuel 2018;215:57–65. https://doi.org/10.1016/J.FUEL.2017.11.019.
[30] Giudicianni P, Gargiulo V, Grottola CM, Alfè M, Ferreiro AI, Mendes MAA, et al. Inherent metal elements in biomass pyrolysis: a review. Energy & Fuels 2021;35:5407–78. https://doi.org/10.1021/ACS.ENERGYFUELS.0C04046.
[31] Giudicianni P, Cardone G, Ragucci R. Cellulose, hemicellulose and lignin slow steam pyrolysis: thermal decomposition of biomass components mixtures. J Anal Appl Pyrolysis 2013;100:213–22. https://doi.org/10.1016/J.JAAP.2012.12.026.
[32] Ma Z, Yang Y, Wu Y, Xu J, Peng H, Liu X, et al. In-depth comparison of the physicochemical characteristics of bio-char derived from biomass pseudo components: hemicellulose, cellulose, and lignin. J Anal Appl Pyrolysis 2019;140:195–204. https://doi.org/10.1016/J.JAAP.2019.03.015.
[33] Byrne CE, Nagle DC. Carbonized wood monoliths—characterization. Carbon N Y 1997;35:267–73. https://doi.org/10.1016/S0008-6223(96)00135-2.
[34] Johnson DJ, Tomizuka I, Watanabe O. The fine structure of lignin-based carbon fibres. Carbon N Y 1975;13:321–5. https://doi.org/10.1016/0008-6223(75)90037-8.

[35] Kane S, Ulrich R, Harrington A, Stadie NP, Ryan C. Physical and chemical mechanisms that influence the electrical conductivity of lignin-derived biochar. Carbon Trends 2021;5:100088. https://doi.org/10.1016/J.CARTRE.2021.100088.
[36] Ahmetli G, Kocaman S, Ozaytekin I, Bozkurt P. Epoxy composites based on inexpensive char filler obtained from plastic waste and natural resources. Polym Compos 2013;34:500–9. https://doi.org/10.1002/PC.22452.
[37] Weber K, Quicker P. Properties of biochar. Fuel 2018;217:240–61. https://doi.org/10.1016/j.fuel.2017.12.054.
[38] Ferrari A, Robertson J. Interpretation of Raman spectra of disordered and amorphous carbon. Phys Rev B Condens Matter Mater Phys 2000;61:14095–107. https://doi.org/10.1103/PhysRevB.61.14095.
[39] Gabhi RS, Kirk DW, Jia CQ. Preliminary investigation of electrical conductivity of monolithic biochar. Carbon N Y 2017;116:435–42. https://doi.org/10.1016/J.CARBON.2017.01.069.
[40] Bartoli M, Giorcelli M, Rosso C, Rovere M, Jagdale P, Tagliaferro A. Influence of commercial biochar fillers on brittleness/ductility of epoxy resin composites. Appl Sci 2019;9:3109. https://doi.org/10.3390/APP9153109.
[41] Manara P, Zabaniotou A. Towards sewage sludge based biofuels via thermochemical conversion – a review. Renew Sustain Energy Rev 2012;16:2566–82. https://doi.org/10.1016/J.RSER.2012.01.074.
[42] Tan Z, Lagerkvist A. Phosphorus recovery from the biomass ash: a review. Renew Sustain Energy Rev 2011;15:3588–602. https://doi.org/10.1016/J.RSER.2011.05.016.
[43] Vassilev SV, Baxter D, Andersen LK, Vassileva CG. An overview of the chemical composition of biomass. Fuel 2010;89:913–33. https://doi.org/10.1016/j.fuel.2009.10.022.
[44] Debiagi P, Gentile G, Cuoci A, Frassoldati A, Ranzi E, Faravelli T. A predictive model of biochar formation and characterization. J Anal Appl Pyrolysis 2018;134:326–35. https://doi.org/10.1016/J.JAAP.2018.06.022.
[45] Megala S, Rekha B, Saravanathamizhan R. Chemical and non-chemical pretreatment techniques for bio ethanol production from biomass. Int J Energy Water Resour 2020;4:199–204. https://doi.org/10.1007/S42108-020-00064-7. 2020 42.
[46] Peng C, Zhang G, Han J, Conversion XLCR. Hydrothermal conversion of lignin and black liquor for phenolics with the aids of alkali and hydrogen donor. undefined. Elsevier n.d; 2019.
[47] Hospodarova V, Singovszka E, Stevulova N, Hospodarova V, Singovszka E, Stevulova N. Characterization of cellulosic fibers by FTIR spectroscopy for their further implementation to building materials. Am J Anal Chem 2018;9:303–10. https://doi.org/10.4236/AJAC.2018.96023.
[48] Grube M, Lin JG, Lee PH, Kokorevicha S. Evaluation of sewage sludge-based compost by FT-IR spectroscopy. Geoderma 2006;130:324–33. https://doi.org/10.1016/J.GEODERMA.2005.02.005.
[49] Boeriu CG, Bravo D, Gosselink RJA, Van Dam JEG. Characterisation of structure-dependent functional properties of lignin with infrared spectroscopy. Ind Crops Prod 2004;20:205–18. https://doi.org/10.1016/J.INDCROP.2004.04.022.
[50] Giudicianni P, Gargiulo V, Alfè M, Ragucci R, Ferreiro AI, Rabaçal M, et al. Slow pyrolysis of xylan as pentose model compound for hardwood hemicellulose: a study of the catalytic effect of Na ions. J Anal Appl Pyrolysis 2019;137:266–75. https://doi.org/10.1016/J.JAAP.2018.12.004.
[51] van Lith SC, Jensen PA, Frandsen FJ, Glarborg P. Release to the gas phase of inorganic elements during wood combustion. Part 2: influence of fuel composition. Energy and Fuels 2008;22:1598–609. https://doi.org/10.1021/EF060613I.
[52] Wei H, Gao B, Ren J, Li A, Yang H. Coagulation/flocculation in dewatering of sludge: a review. Water Res 2018;143:608–31. https://doi.org/10.1016/J.WATRES.2018.07.029.
[53] Tuinstra F, Koenig JL. Raman spectrum of graphite. J Chem Phys 2003;53:1126. https://doi.org/10.1063/1.1674108.
[54] Leng L, Yang L, Chen J, Leng S, Li H, Li H, et al. A review on pyrolysis of protein-rich biomass: nitrogen transformation. Bioresour Technol 2020;315:123801. https://doi.org/10.1016/J.BIORTECH.2020.123801.
[55] Yuan T, He W, Yin G, Xu S. Comparison of bio-chars formation derived from fast and slow pyrolysis of walnut shell. Fuel 2020;261:116450. https://doi.org/10.1016/J.FUEL.2019.116450.
[56] Yang J, Mori T, Kuwabara M. Mechanism of carbothermic reduction of hematite in hematite–carbon composite pellets. ISIJ Int 2007;47:1394–400. https://doi.org/10.2355/ISIJINTERNATIONAL.47.1394.
[57] Hoch LB, Mack EJ, Hydutsky BW, Hershman JM, Skluzacek JM, Mallouk TE. Carbothermal synthesis of carbon-supported nanoscale zero-valent iron particles for the remediation of hexavalent chromium. Environ Sci Technol 2008;42:2600–5. https://doi.org/10.1021/ES702589U/SUPPL_FILE/ES702589U-FILE004.PDF.
[58] Trubetskaya A, Jensen PA, Jensen AD, Garcia Llamas AD, Umeki K, Glarborg P. Effect of fast pyrolysis conditions on biomass solid residues at high temperatures. Fuel Process Technol 2016;143:118–29. https://doi.org/10.1016/J.FUPROC.2015.11.002.
[59] Niksa S. Predicting the rapid devolatilization of diverse forms of biomass with bio-flashchain. Proc Combust Inst 2000;28:2727–33. https://doi.org/10.1016/S0082-0784(00)80693-1.
[60] Solimene R, Cammarota A, Chirone R, Leoni P, Rossi N, Salatino P. Devolatilization and fragmentation of solid lignin-rich residues from bioethanol production in lab-scale fluidized bed reactors. Chem Eng Trans 2016;50. https://doi.org/10.3303/CET1650014.
[61] Troiano M, Cammarota A, Tregambi C, Chirone R, Salatino P, Solimene R. Fluidized bed combustion of solid lignin-rich residues from bioethanol production. Powder Technol 2020;371:170–9. https://doi.org/10.1016/J.POWTEC.2020.05.070.
[62] Tregambi C., Montagnaro F., Salatino P., Solimene R. Solar-driven torrefaction of a lignin-rich biomass residue in a directly irradiated fluidized bed reactor. 2019;191:1609–27. 10.1080/00102202.2019.1607847.
[63] Zhang L, Yang X, Dongdong F, Duan F, Wang P. Grindability, thermogravimetric characteristics, and kinetics analysis of semi-biochar from coarse wood pyrolyzed in a fluidized bed. Asia-Pacific J Chem Eng 2020;15:e2458. https://doi.org/10.1002/APJ.2458.
[64] Sh L, Lee BH, Jeong TY, Jeon CH. Effects of different pretreatment methods on the grindability of pitch pine sawdust biomass and its blends with coal. J Mech Sci Technol 2020;34:2235–43. https://doi.org/10.1007/S12206-020-0445-4. 2020 345.
[65] Jing X, Zhao W, Lan L. The effect of particle size on electric conducting percolation threshold in polymer/conducting particle composites. J Mater Sci Lett 2000;19:377–9. https://doi.org/10.1023/A:1006774318019. 2000 195.
[66] Ayadi R., Koubaa A., Braghiroli F., Migneault S., Wang H., Bradai C. Effect of the pyro-gasification temperature of wood on the physical and mechanical properties of biochar-polymer biocomposites. MdpiCom n.d. 10.3390/ma13061327.